

Article

X-Band Active Phased Array Antenna Using Dual-Port Waveguide for High-Power Microwave Applications

Rong Liu ¹, Naizhi Wang ^{1,2,*}, Tong Li ¹, Ruoqiao Zhang ¹ and Hongchao Wu ^{1,2}¹ The 14th Research Institute of China Electronics Technology Group Corporation, Nanjing 210039, China² Science and Technology of Antenna and Microwave Laboratory, Nanjing 210039, China

* Correspondence: nzwang@163.com

Abstract: An X-band active phased array horn antenna with high power capacity and high peak power is proposed in this paper. At the horn aperture, the baffles are loaded to suppress higher-order modes and eliminate blind spots during beam scanning. Straight walls are added to improve impedance matching. Considering that the peak power that T/R modules can provide is very limited, the proposal of a dual-port waveguide breaks through the bottleneck of the power capacity of a single-port input for the first time. The proposed curved dual-port waveguide is used to connect the horn antenna and the T/R module, which is verified to improve the power capacity of the overall internal structure. Simulated and measured results show that $VSWR \leq 2$ in the frequency range of 7.5–8.5 GHz. There is no grating lobe in the $\pm 10^\circ$ scanning range and the maximum gain drop does not exceed 0.4 dB. The power capacity of the proposed HPM array is 56.34 MW. The phased array antenna has the characteristics of flexible scanning, small size, and high gain, and can be applied in high-power microwave systems.

Keywords: high-power microwave; active phased array; power capacity; beam scanning; curved dual-port waveguide



Citation: Liu, R.; Wang, N.; Li, T.; Zhang, R.; Wu, H. X-Band Active Phased Array Antenna Using Dual-Port Waveguide for High-Power Microwave Applications. *Electronics* **2022**, *11*, 4064. <https://doi.org/10.3390/electronics11234064>

Academic Editor: Reza K. Amineh

Received: 17 November 2022

Accepted: 2 December 2022

Published: 6 December 2022

Publisher's Note: MDPI stays neutral with regard to jurisdictional claims in published maps and institutional affiliations.



Copyright: © 2022 by the authors. Licensee MDPI, Basel, Switzerland. This article is an open access article distributed under the terms and conditions of the Creative Commons Attribution (CC BY) license (<https://creativecommons.org/licenses/by/4.0/>).

1. Introduction

High-power microwave (HPM) can be effectively used in electronic countermeasures, high-power radar, and high-power transmission [1–3]. The transmitting antenna is an important device in a high-power microwave system. Researchers in related fields are used to dividing the high-power microwave antenna into three aspects, including the coaxial beam-rotating antenna (COBRA), the mode conversion antenna, and the high peak power antenna with a mode converter. The COBRA [4–6] has a simple structure and a high power capacity, but it is reported that it is difficult to synthesize beams in HPM arrays. The mode conversion antenna [7] is regarded as a special structure that integrates the functions of the mode converter and the antenna. This kind of HPM antenna simplifies the transition structure connected to the high-power microwave source and converts the transmission mode that cannot be radiated into the axial radiation mode. However, its HPM antenna has the defects of huge size and single-aperture radiation, so it is difficult to be used in high-frequency microwave devices. Common HPM antennas with a mode converter include Vlasov antennas [8–10], helical antennas [11–13], leaky waveguide antennas [14–17], horn antennas [18–25], parabolic reflector antennas [26,27], all-metal antenna [28,29] and EZ antennas [30,31]. The Vlasov antenna can generate a narrow radiation beam by configuring different circular waveguide opening shapes with a parabolic cylindrical reflector. Due to its narrow radiation beam, its radiation characteristics will be limited when forming an antenna array. The HPM helical antenna can be designed as an axial mode helical antenna unit or as a phase shifter on a reflector plate due to its simple configuration and small-sized mode conversion structure. However, the feed horn of the helical antenna array blocks the radiation of the main beam during beam scanning. In addition, the parabolic reflector

antenna also has similar problems. The leaky waveguide antenna and slot antenna are considered to be able to achieve a small antenna size and a high power capacity, but their beams can only be scanned in one dimension. The horn antenna is widely used in HPM due to its high power capacity, simple structure, and convenient configuration. The horn antenna proposed in [13] has a large aperture, which is not conducive to integration and power synthesis.

Due to historical development problems, compared with plasma physics and pulsed power technologies, high-power microwaves are relatively less integrated with traditional microwave technologies. Many technologies of traditional microwave antennas have not been effectively applied to high-power microwaves. There are few reports at home and abroad on the introduction of phased array antenna technology into HPM transmission systems. The phased array has the advantages of flexible beam scanning, low side lobes, easy array formation, convenient disassembly and maintenance, and high mobility, which can make up for the shortcomings of existing HPM antennas.

Combining the flexible beam scanning of phased array and the high power capacity of the horn antenna, a new type of HPM array antenna is proposed for the first time. Different from other horn antennas, the proposed horn antenna reconfigures the radiation structure of the aperture plane. The added straight wall effectively matches the impedance value of the free space and the antenna. The proposed partition plate inhibits the generation of higher-order modes. In addition, this paper innovatively proposes a curved dual-port waveguide to transmit high power. The waveguide improves the overall power capacity of the active phased array, reduces the overall profile height, and reduces the power value required by T/R modules. Compared with the traditional rectangular waveguide, this waveguide has a more compact structure and superior power transmission efficiency. The active phased array using the HPM horn antenna and dual-port waveguide configuration shows good beam scanning characteristics and high peak power advantages and is proven to have HPM application value.

The structure of this paper is organized as follows. The research status and comparison with HPM antennas have been reported above in Section 1. In Section 2, the geometry of the HPM antenna is introduced. The horn antenna and the dual-port waveguide are configured. In particular, power capacity is emphasized. In Sections 3 and 4, the simulation and measurement results of the HPM active phased array antenna are presented, respectively. In Section 5, the advantages and application value of the proposed antenna are described through the comparison of existing research, and then the follow-up work is prospected. The conclusion is presented in Section 6.

2. The 1×8 Array Antenna Design

Figure 1 shows the geometry of a high-power microwave 1×8 phased array and antenna unit proposed in this paper, which consists of high-gain horns and two side-by-side rectangular waveguides for feeding. Since the antenna array proposed is under the active phased array system, the rear end of each antenna element is connected to an independent T/R component and feed. After the T/R module, two rectangular waveguide ports are input with equal amplitude and phase. The transmitted electromagnetic field is merged at the ends of the dual-port waveguide and passed through the curved waveguide structure. Finally, the energy is radiated into free space through a high-gain pyramid horn connected to a rectangular waveguide. At the same time, the size of the rectangular waveguide is the same as the unit spacing of the antenna, which acts as a metal reflector to prevent the energy from being reflected into the system and causing damage to the microwave device. The detailed dimensions of the proposed HPM unit and curved waveguide are listed in Table 1.

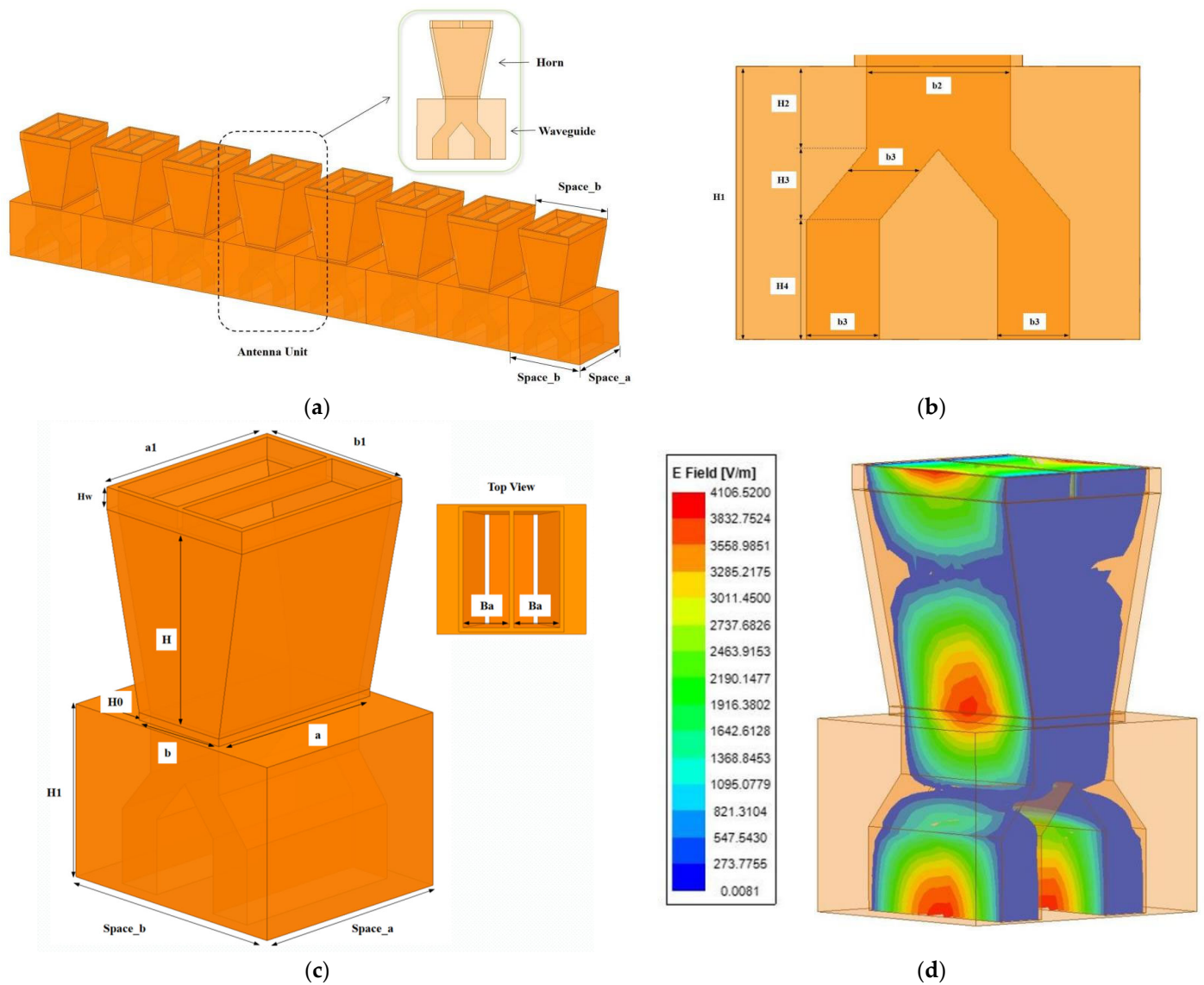


Figure 1. The geometry of the HPM phased array antenna: (a) the 3D model of the 1×8 array antenna, (b) the model of the curved waveguide, (c) the 3D model of the HPM phased array antenna unit, and (d) the field strength distribution of the HPM antenna unit.

Table 1. Detailed dimensions of the antenna unit (unit: mm).

Parameter	Value	Parameter	Value
a	26.86	b	14.16
a1	28.5	b1	24
H	26	H1	20
Hw	3	Ba	10.5
H0	1	H2	6
H3	4	H4	10
b2	12.16	b3	6.08

Figure 1b,c show the geometry of the curved waveguide and antenna element, respectively. Considering the working frequency band range of the proposed antenna and the volume size of the rear T/R module it is recommended that the antenna unit spacing Space_a is 34 mm and Space_b is 29.5 mm.

Figure 1d shows that the maximum field strength value, E_{max} , of the antenna unit is 4106.52 V/m. The proposed antenna unit is an all-metal structure, and does not need to be sealed or filled with inert gas, so the breakdown voltage inside the antenna in air, E , is 3×10^6 V/M. The power capacity, P , can be obtained by substituting the parameters into Equation (1), and is 533.69 kW. In Equation (1), E is the air breakdown field strength value, E_{max} is the maximum field strength value of the antenna unit, P_{in} is the input power value of the antenna feed end, and P_{in} is taken as 1 W in this paper [12].

$$P = \left(\frac{E}{E_{max}} \right)^2 P_{in} \tag{1}$$

2.1. The Horn Design

During beam scanning, the air impedance will change with the different beam scanning angles, as shown in Equations (1) and (2), so when the scanning angle increases, the impedance matching at the horn aperture will deteriorate. The reconfiguration of the horn aperture surface is considered to affect the distribution of the radiated electromagnetic field at the contact surface with the free space, especially the new capacitance and reactance brought about by the change of the scanning angle, which will be regarded as the improvement advantage of the HPM horn proposed in this paper and will be emphasized. To study the scanning standing wave characteristics of the horn antenna, an analytical model of the antenna element under the periodic boundary condition, as shown in Figure 2, is established.

$$Z_{TE} = \sqrt{\frac{\mu_0}{\epsilon_0}} \sec \theta \tag{2}$$

$$Z_{TM} = \sqrt{\frac{\mu_0}{\epsilon_0}} \cos \theta \tag{3}$$

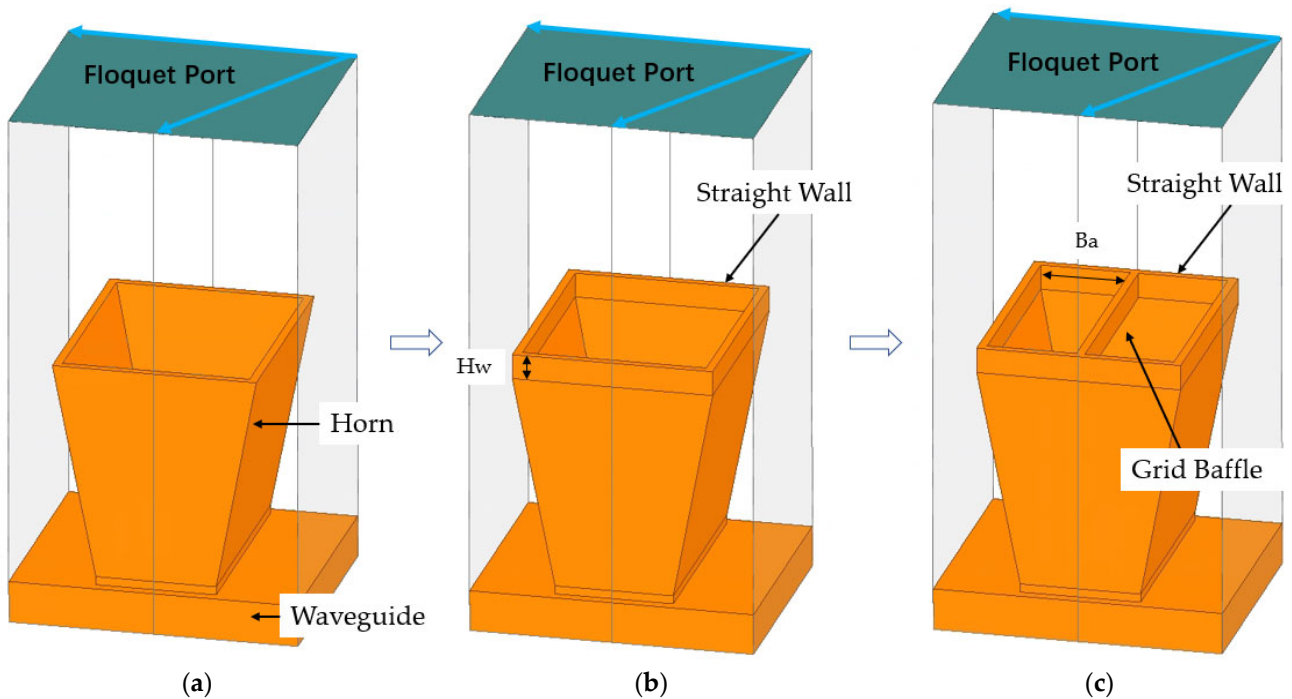


Figure 2. Design evolution of the HPM antenna unit consisting of a horn and a waveguide: (a) the basic antenna unit, (b) adding a straight wall to the horn radiator, and (c) adding a grid baffle at the center of the straight wall.

Figure 2 shows that the straight sidewall and grid baffle configured at the horn aperture are two evolutions of the antenna element geometry. A straight wall with variable length Hw is loaded at the horn aperture to improve the impedance matching to ensure that the impedance at the horn aperture can still match the air impedance when the scanning angle is large, as in Figure 2b.

The effect of the change of the scanning angle on the impedance of the radiation-free space can be obtained by observing the impedance change of the Floquet port. Since the impedance of the free space is not related to the frequency and the impedance of the antenna element will decrease with the increase of the frequency, the impedance matching at the center frequency point is mainly considered in the design. When the scanning angle increases, the mutual coupling effect between the units increases and the aperture surfaces of other surrounding horn antennas will leak electromagnetic fields to the horn unit. Excess inductance and reactance will be generated at the horn aperture surface. The sidewall of the horn antenna can restrain the leakage of the electromagnetic field to a certain extent. The change reflected in the equivalent circuit is to reduce the inductance value, L , generated by the surface current. The resonant frequency is inversely proportional to the inductance term in the equivalent circuit, which indicates that the longer the straight wall length, H , is, the lower the resonant frequency point is. This can be observed in the frequency band characteristic analysis in Figure 3. Adjust the value of H to set the operating frequency of the horn antenna within the required operating range, which plays a role in adjusting the impedance of the resonant point.

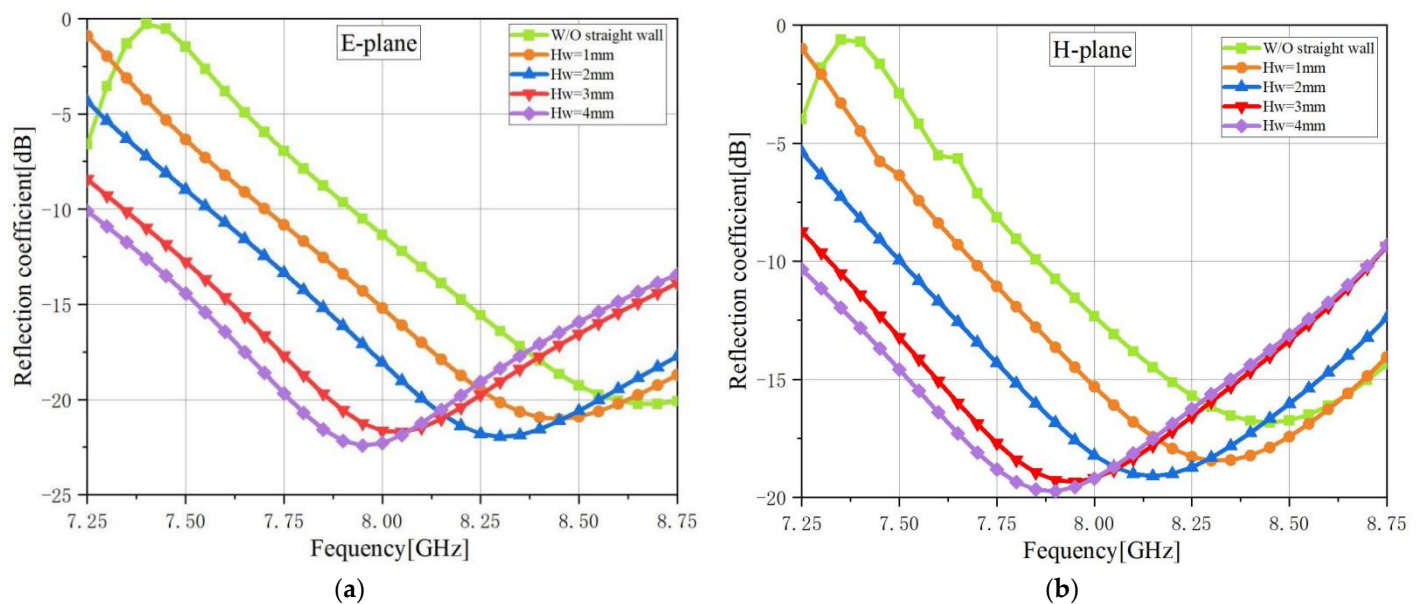


Figure 3. The comparison of the active S_{11} before and after loading the metal sidewall when the scan angle is $\pm 10^\circ$: (a) E-plane and (b) H-plane.

However, when sidewalls are added to the horn aperture, higher-order modes will inevitably be introduced, which will lead to the deterioration of the pattern. The diaphragm is arranged in the middle of the long side of the sidewall, which is considered able to suppress the high-order mode formed, eliminate the blind spot during scanning, and improve the active standing wave during beam scanning.

Figure 4a shows the surface current distribution at the horn aperture with the grid baffle added. The Floquet mode of the electromagnetic simulation software HFSS is used to analyze the influence of high-order modes on the antenna, especially the surface current distribution at the horn aperture under different high-order modes. The attenuation of high-order modes is affected by the wide boundary value, b , of the horn aperture. In this paper, the addition of a separator changes the size of the wide boundary value, b , thus

indirectly changing the boundary conditions of the transmission mode, which is in cut-off mode for higher modes.

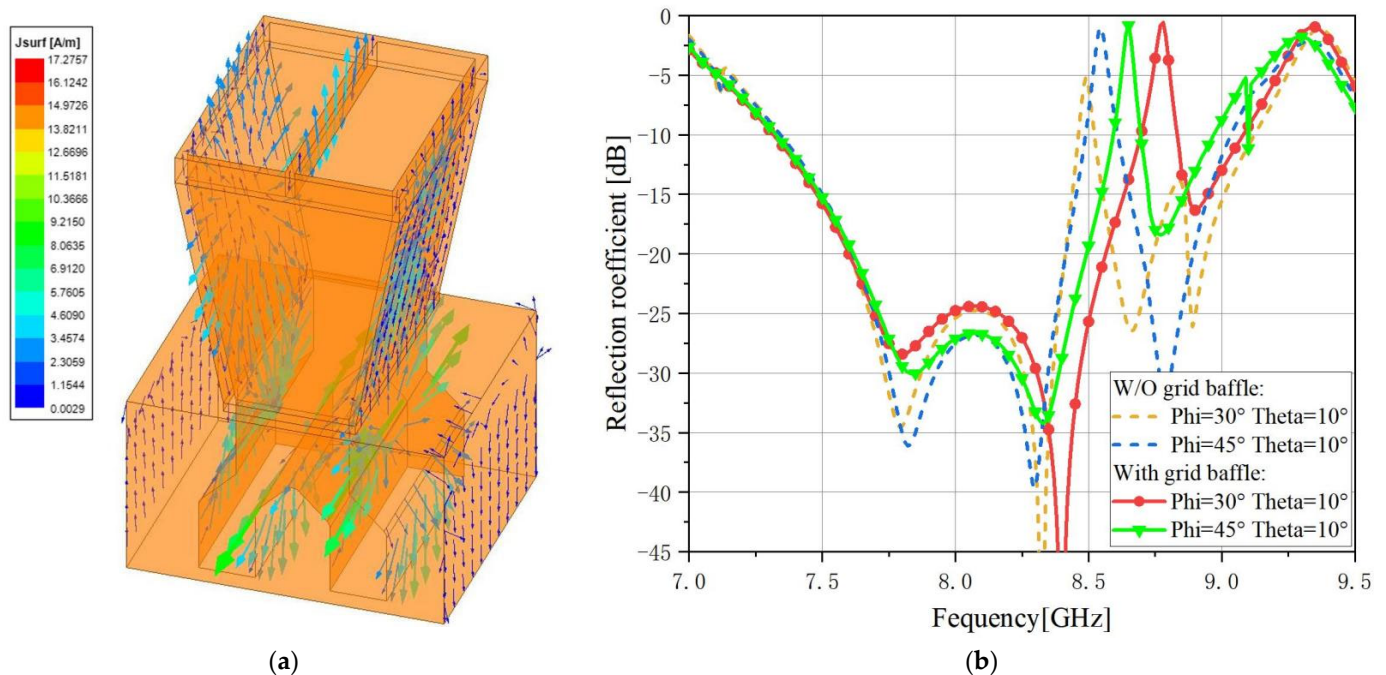


Figure 4. (a) The surface current distribution at the horn aperture with the grid baffle added. (b) The active reflection coefficients before and after adding the grid baffle.

Figure 4b shows the active reflection coefficients before and after adding the grid baffle at different scanning angles. It can be observed that the reflection coefficient in the high-frequency band is larger before adding a grid baffle on the straight wall of the horn antenna unit. When the scanning angle is $\Phi = 30^\circ$, the reflection coefficient at the frequency of 8.5 GHz sharply deteriorates, which is considered a scanning blind spot that can be verified in the far-field pattern. Similarly, when the scanning angle is $\Phi = 45^\circ$ and $\Theta = 10^\circ$, the frequency point of 8.55 GHz is also observed as a scanning blind spot. The added grid baffle eliminates the scanning blind spot and improves the active standing wave. In addition, the gain at the original blind spot is also increased by 0.2 dB after adding the grid baffle.

2.2. Curved Waveguide

Figure 5 shows the evolution of the geometric design of the curved waveguide proposed in this paper. After considering the purpose of improving the transmission power and efficiency of the array, the rectangular WG-1 with the initial geometry of a feed channel Port1 is changed to a rectangular WG-2 configured with dual ports Port1 and Port2 with the same transmission phase and amplitude. However, this change will increase the length of the rectangular waveguide, and the two ports are too close to each other, which may lead to short-circuiting during connection. In this regard, a novel curved waveguide is proposed to transmit TE_{10} mode fields with high power. Compared with WG-2, the middle section of WG-3 is bent, which makes it possible to reduce the waveguide length. Figure 6 shows the active reflection coefficient of the antenna unit under three different waveguide geometric configurations.

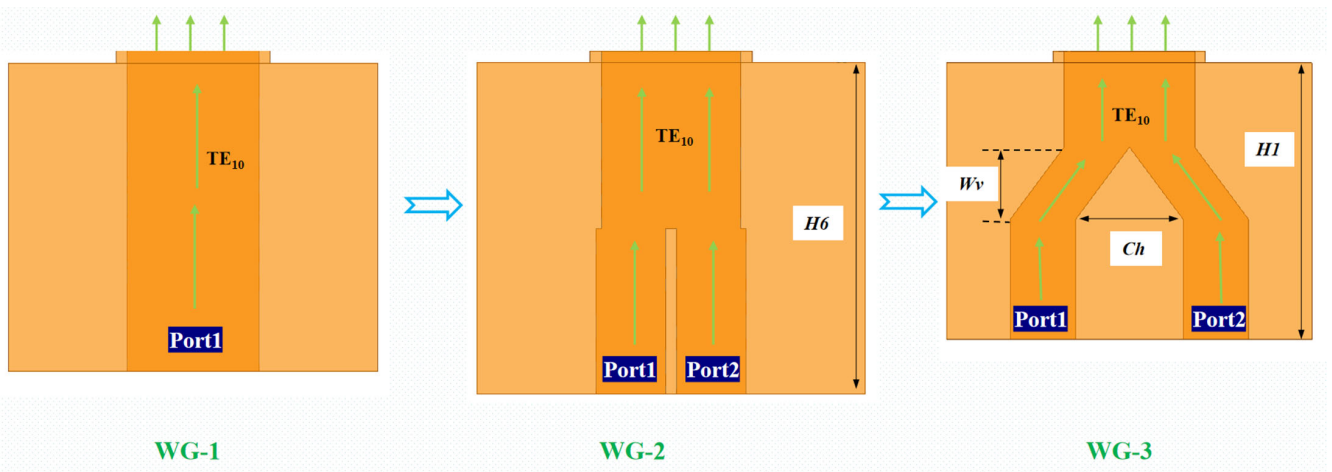


Figure 5. The evolution of the geometric design of the curved waveguide.

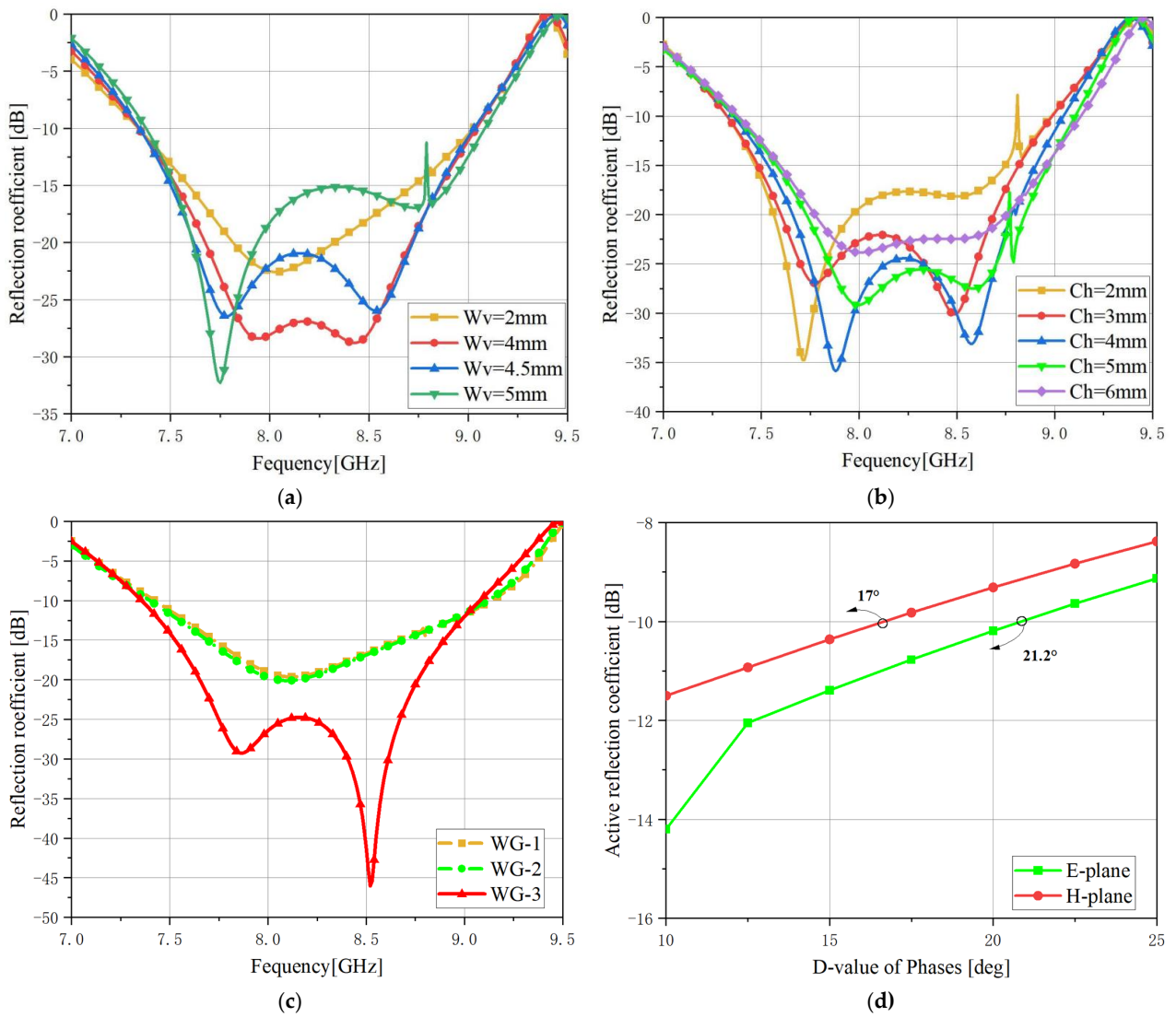


Figure 6. (a) The sensitivity analysis of parameter Wv , (b) the sensitivity analysis of parameter Ch , (c) the reflection coefficient of the curved waveguide, and (d) the reflection coefficient with the different D-values of phases.

The discussion of WG-2 and WG-3 can explain the impedance matching of the proposed antenna. The geometry of WG-3 has an additional section of waveguide in the middle, that is, a bent waveguide, compared with WG-2. The values of parameters Ch and Wv determine the geometry of the bent waveguide, which further affects the impedance of the bent waveguide. The impedance value of the curved waveguide is between the impedance value of the port and the horn, which acts as the impedance transition section. The sensitivity analysis of parameters Ch and Wv in Figure 6a,b also shows their regulating effect on impedance matching. Finally, the optimized values $Ch = 4$ mm and $Wv = 4$ mm are selected.

Figure 6c shows the active reflection coefficient of the antenna unit under three different waveguide geometric configurations. Since the designed waveguide is fed by two ports, the experimental results of the passive standing wave in the measurement of the standing wave ratio do not consider the influence of another port on the reflection coefficient, so the results of the active standing wave ratio are considered more convincing. In the infinite array of the active phased array, the reflection coefficient of WG-3 is smaller than that of WG-1 and WG-2 in the frequency band. The length parameter H1 of WG-3 is 20 mm, and the length parameter H6 of WG-1 is 30 mm. The profile height of the waveguide is 33.3% lower than before. Furthermore, the input power of WG-3 is twice that of WG-1, which can effectively improve the power. The introduction of the curved waveguide not only reduces the profile height, but also realizes the impedance matching between the horn antenna and the waveguide. Obviously, impedance matching can avoid the concentration of field strength inside the waveguide, thus reducing the maximum field strength value, and further improving the power capacity.

The influence of the phase imbalance of the two ports on the reflection coefficient and power capacity is worthy of further verification. At the HPM antenna array, take different values for the phases of Port1 and Port2 to make their difference between 0° and 25° , to observe the transformation of the reflection coefficient and power capacity. As shown in Figure 6d, when the scanning angle is $\pm 10^\circ$, the reflection coefficient of E-plane scanning is greater than -10 dB after the phase difference between the two ports exceeds 17° , which is considered ineffective. Similarly, when the phase difference between the two ports exceeds 21.2° , the imbalance of the ports will be regarded as an unavoidable problem. This analysis requires that the phase difference of the Tx module during power feeding should be controlled within an acceptable range, which can be reached by the current T/R module performance.

Figure 7 shows that in the simulation experiment, the power capacity of WG-1 and WG-3 has a small difference. The reason for selecting WG-3 is that the actual input power cannot reach the simulated power capacity due to the limitation of the power amplitude value of the back-end active T/R module itself, which is verified that the power capacity can only reach half of the simulated power in the actual array formation. Using a dual-port waveguide to input power can solve this problem and can greatly reduce the power value that the back-end components need to provide, which shows that WG-3 has more practical high-power microwave application value.

2.3. Power Capacity

Figure 8 shows the field distribution of the HPM antenna unit. To improve the power capacity, it is necessary to consider the power loss on the transmission path of the TE_{10} mode field and minimize the concentration of field strength at the discontinuous boundary. The boundary condition of electric field is changed at the bend and intersection of the sidewall of the dual-port waveguide.

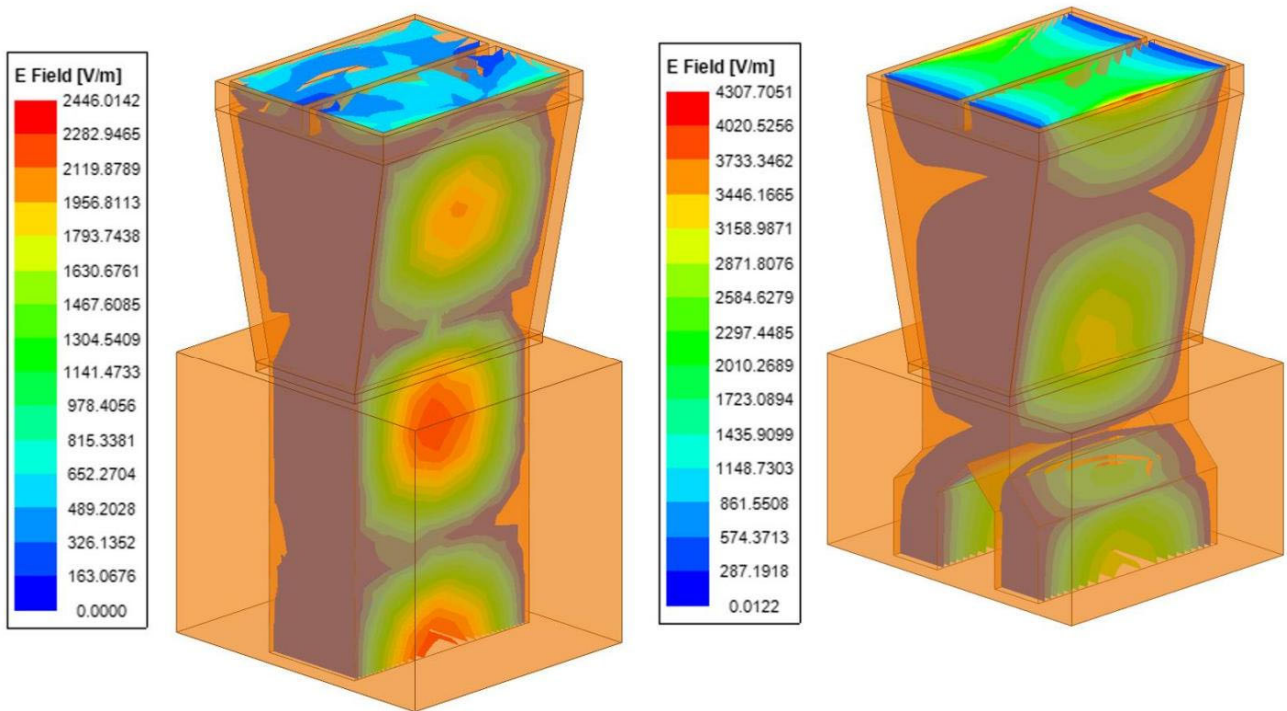


Figure 7. The field distribution of WG-1 and WG-3.

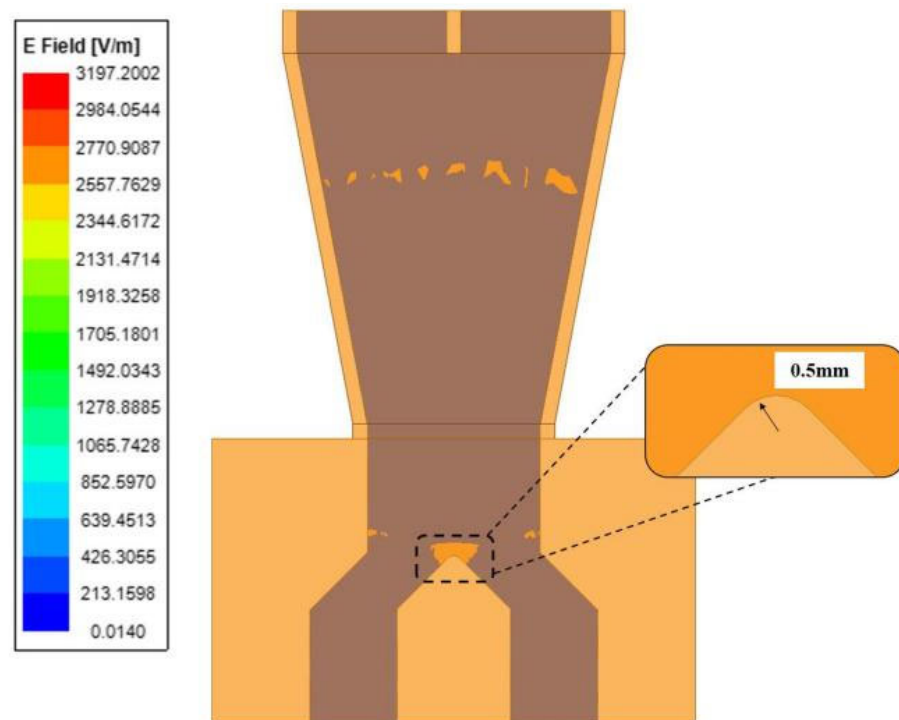


Figure 8. The field distribution of the HPM antenna unit.

The field distribution near the waveguide is very sensitive to the power capacity, especially at the junction of two ports. As shown in Figure 8, the inner wall of the original WG-3 has an acute angle-shaped discontinuity, which will result in a concentrated electric field at its corner. An unnecessarily large electric field concentration will affect the value of the maximum field strength, which will lead to the reduction of power capacity. Rounding the inner wall will improve the power capacity to a certain extent. However, it must be

pointed out that the grid baffle inevitably causes the concentration of the field strength value, leading to the increase of the maximum field strength value. Finally, when the input power of the two ports is 0.5 W, the maximum field strength, E_{\max} , is 3197.3 V/m. The power capacity can be calculated by Equation (4), where P_{in} is the input power value and E is the air breakdown voltage, which is 3×10^6 V/m. The power capacity of the HPM antenna unit is 880.44 kW and the power capacity of the HPM 8×8 antenna array antenna is 56.34 MW.

$$P = \left(\frac{E}{E_{\max}} \right) P_{\text{in}} \quad (4)$$

3. The 8×8 Array Design

Figure 9 shows the model of the 8×8 antenna array for the high-power microwave and the corresponding fabricated antenna. The entire array is made of all-metal, and the thickness of the horn antenna element is 1 mm. The triangular array is selected as the formation method, and the maximum scanning angle is obtained by substituting the spacing $dx = 29.5$ mm and $dy = 17$ mm according to Equation (5). Considering the actual antenna processing error and the influence of impedance matching, the maximum scanning angle, θ_{\max} , is $\pm 10^\circ$.

$$\sqrt{\left(\frac{\lambda}{2d_x} \right)^2 + \left(\frac{\lambda}{2d_y} \right)^2} = 1 + \sin \theta_{\max} \quad (5)$$

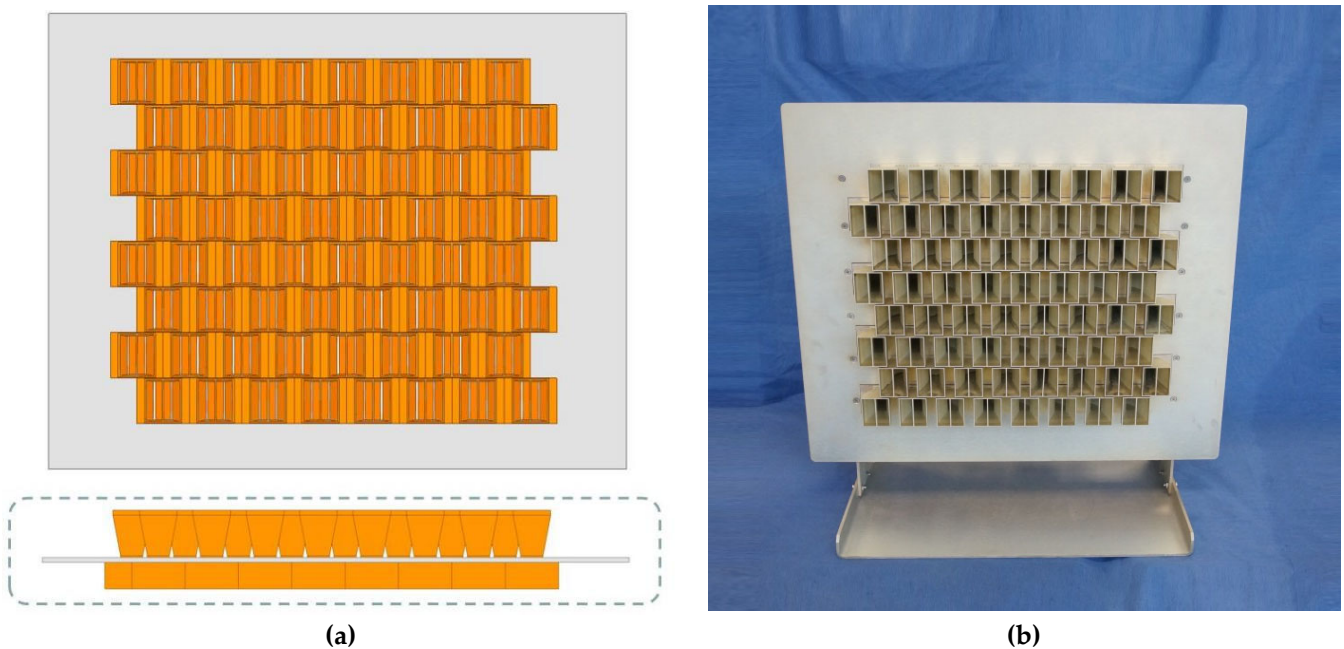


Figure 9. The geometry of the 8×8 phased array antenna: (a) simulated model and (b) manufactured model.

Figure 10 shows the active reflection coefficient of the simulation model at different scanning angles. In the frequency band range of 7.5–8.5 GHz, the active reflection coefficient ≤ -10 dB when the array is scanned in a two-dimensional plane containing the E-plane and the H-plane. The impedance matching between the proposed high-gain horn antenna and the curved dual-port waveguide is verified by this good reflection coefficient result. The size of the horn aperture and the curved waveguide proposed in this paper are suggested to be used as a reference for establishing the HPM array antenna model. According to the simulation results shown in Figure 11, the maximum gain of the array antenna at 7.5, 8, and 8.5 GHz is 27.5, 27.7, and 27.9 dB, respectively. When the main beam of the array antenna is scanned to the maximum angle, the maximum gain attenuation does not exceed

0.4 dB and the pattern grating lobe is not observed. The far-field simulation results of the overall HPM antenna meet the expected high-gain radiation and beam scanning indicators. In addition, the simulation results show that the efficiency of the horn antenna unit is close to 1. Furthermore, the total efficiency of the HPM array is 87.5%, which means that the antenna has the advantages of low loss and high directivity.

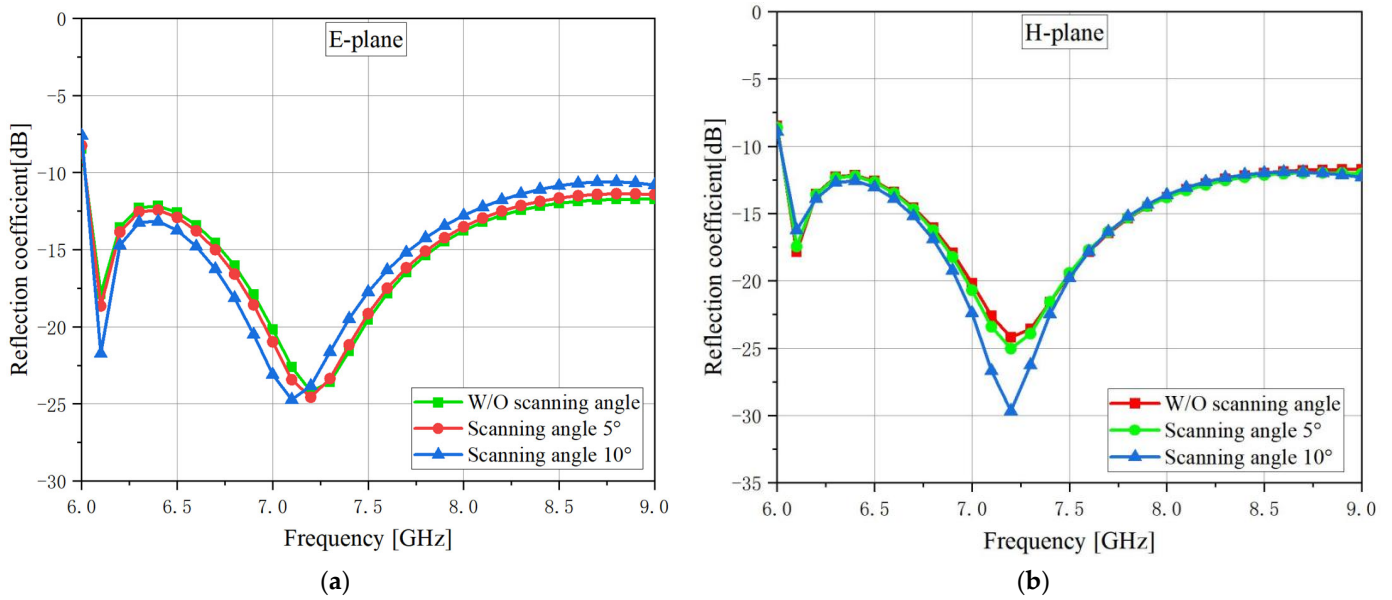


Figure 10. Active VSWR of the 8 × 8 antenna array for the high-power microwave: (a) E-plane and (b) H-plane.

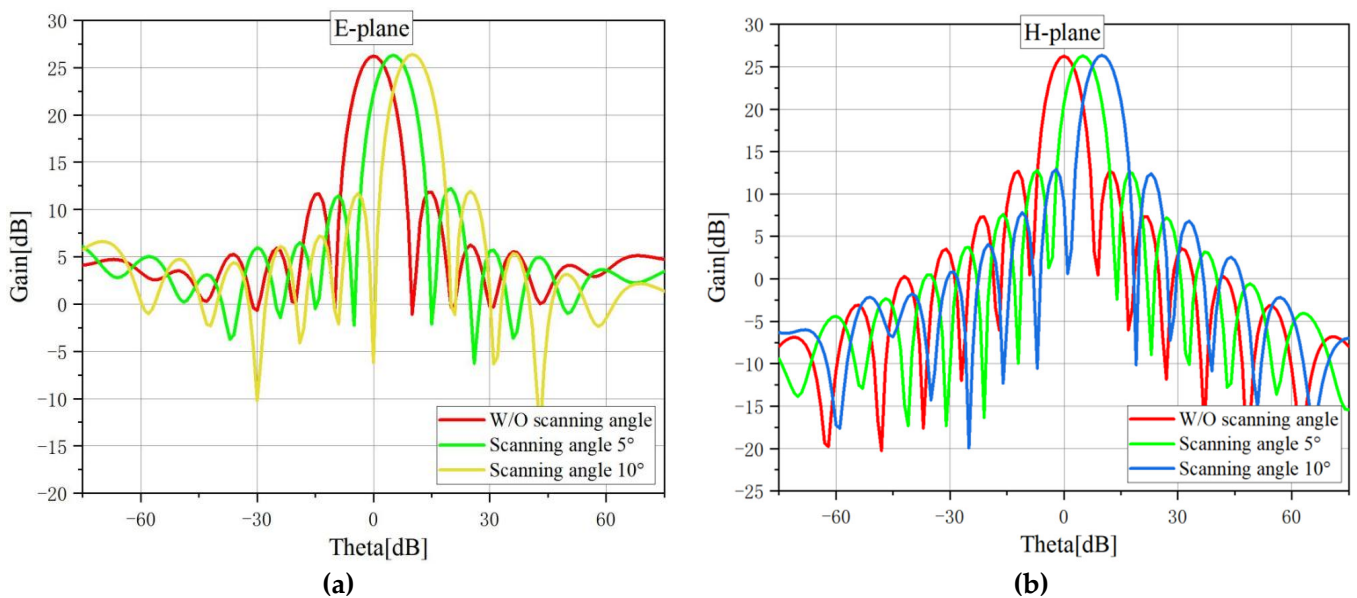


Figure 11. Cont.

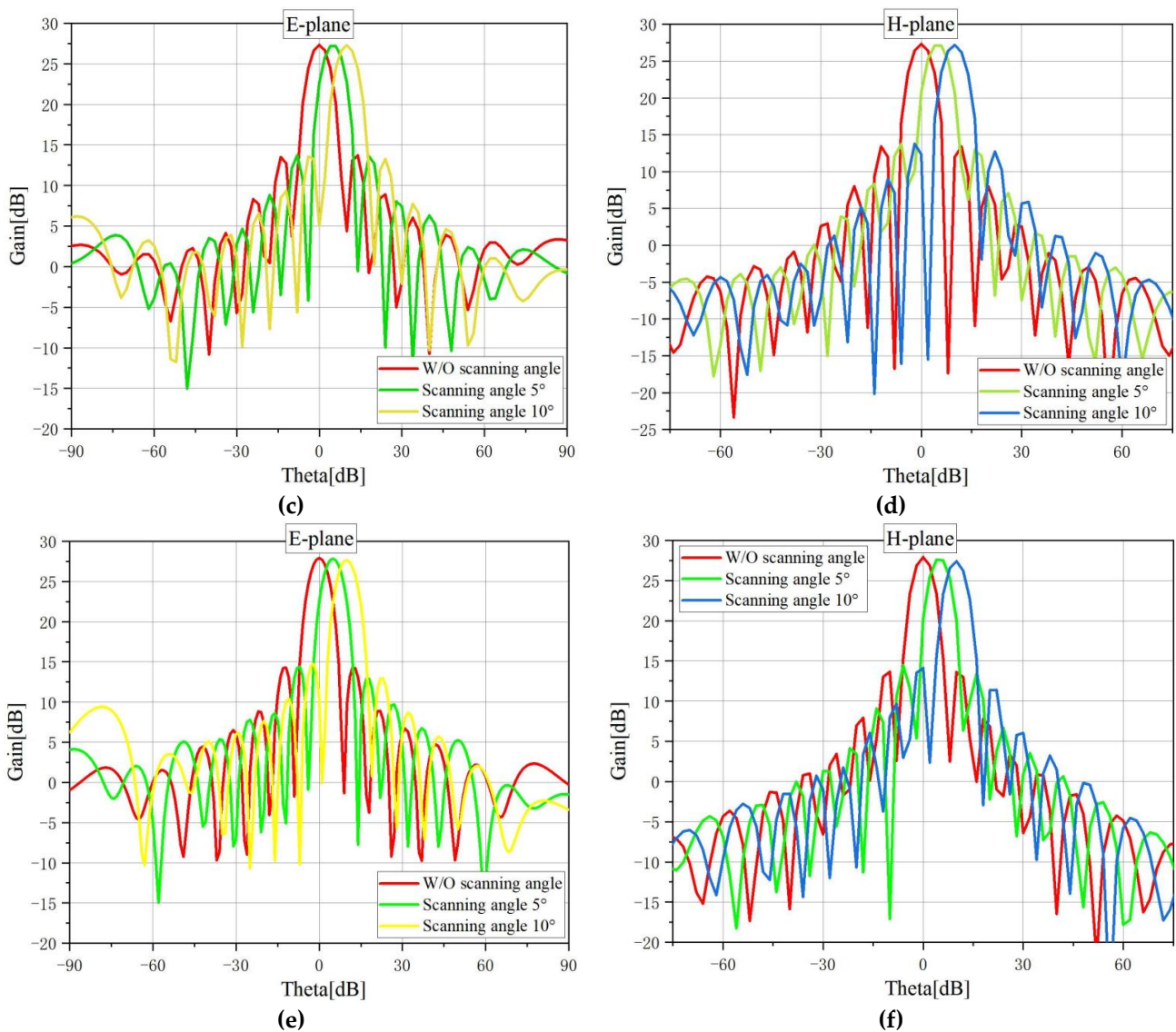


Figure 11. The simulated gain of the proposed 8×8 phased array antenna: (a) E-plane at 7.5 GHz, (b) H-plane at 7.5 GHz, (c) E-plane at 8 GHz, (d) H-plane at 8 GHz, (e) E-plane at 8.5 GHz, and (f) H-plane at 8.5 GHz.

4. Experimental Results

Figure 12 shows the photograph of the assembled HPM 8×8 array antenna. The far-field radiation performance of the HPM antenna at different frequencies was tested in an anechoic chamber. The antenna array is made of all-metal aluminum, and a certain amount of conductive adhesive is coated on the contact point and surface with the connector to ensure good contact and prevent air breakdown.

Figure 13 shows the simulated and measured reflection coefficients of the HPM horn antenna unit. Figure 14 shows the simulated and measured gain of the proposed antenna unit. The experimental data show that there is little difference between the two results. In the frequency range of 7.5–8.5 GHz, the gain of the antenna unit is always no less than 8.4 dB. With the increase of frequency, the gain value of the HPM antenna also increases. Figures 15–17 show the active VSWR of the HPM array antenna at different scanning angles. In the frequency band, the active VSWR is less than 2, which shows that the configuration of antenna elements improves the standing wave characteristics and reduces the reflection coefficient. Thanks to high-precision antenna fabrication, the measured results are in good agreement with the simulation results.

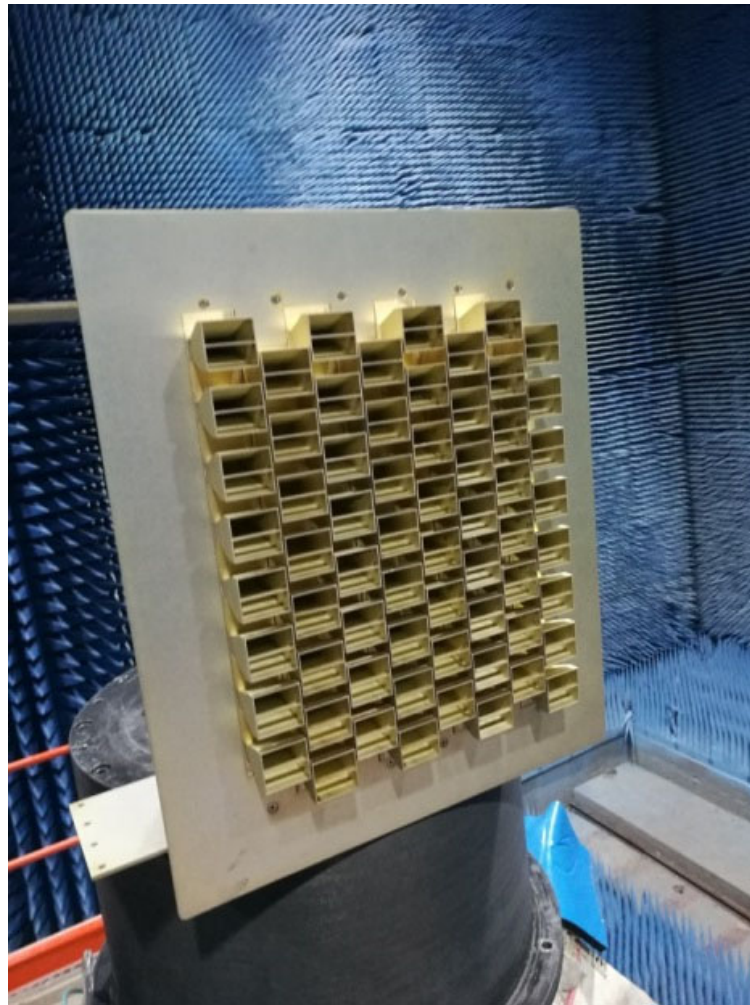


Figure 12. Photograph of the assembled antenna.

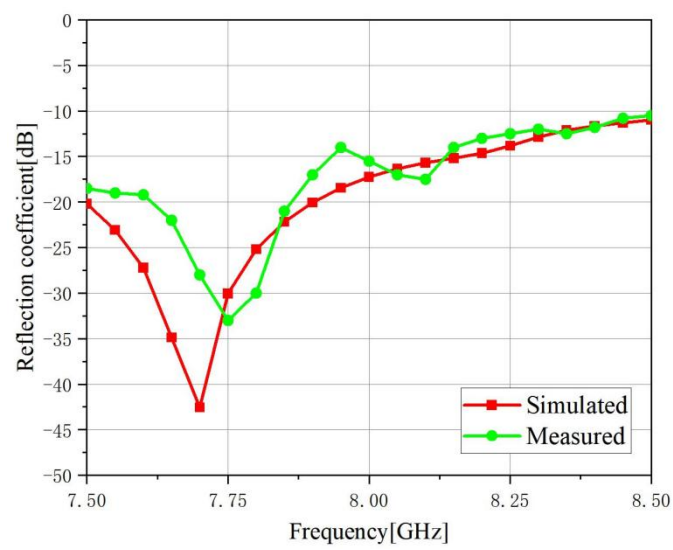


Figure 13. The reflection coefficients of the HPM antenna unit.

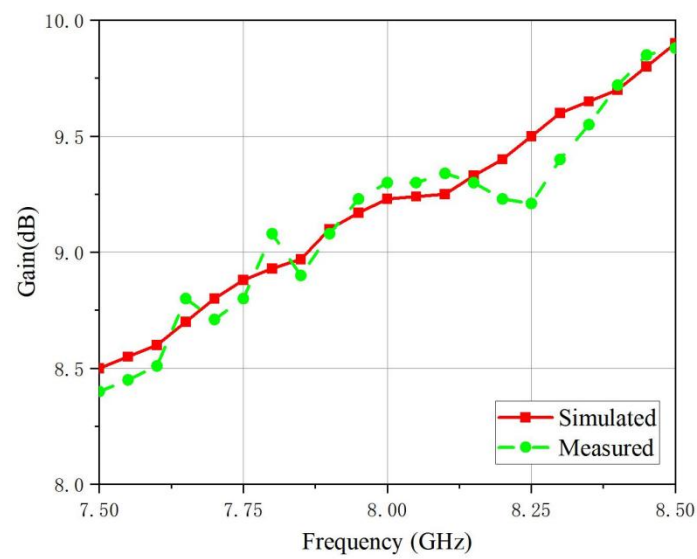


Figure 14. The simulated and measured gain of the HPM unit.

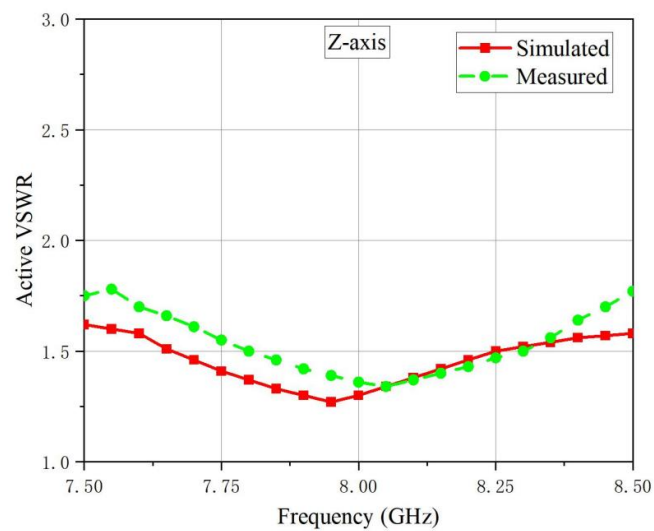


Figure 15. The active VSWR of the Z-axis direction.

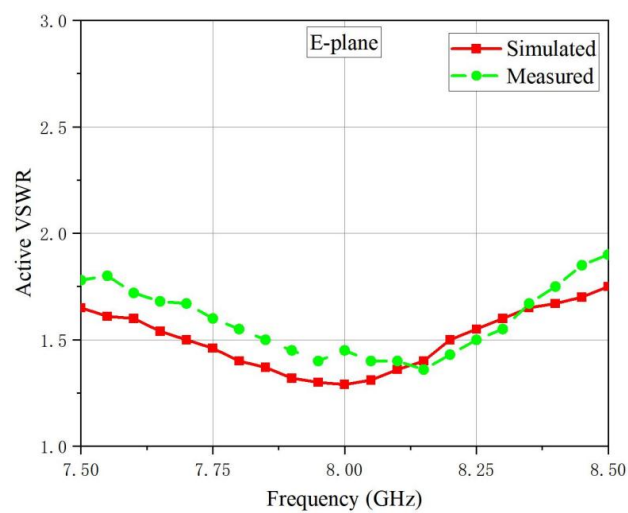


Figure 16. The active VSWR of the E-plane.

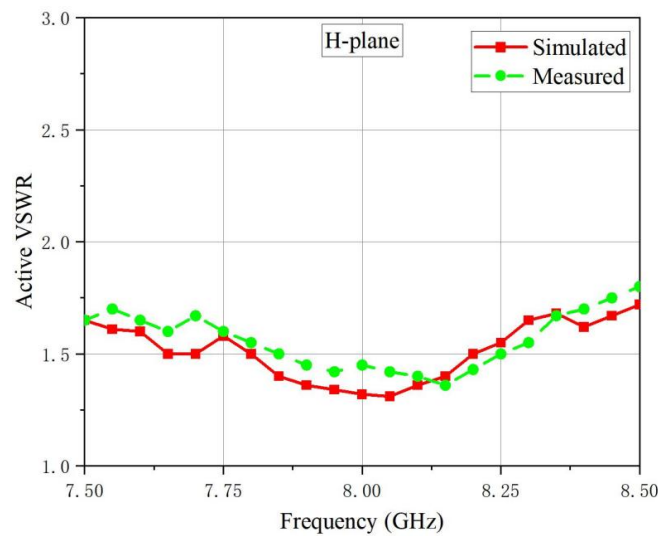


Figure 17. The active VSWR of the H-plane.

5. Discussion

The performances of the proposed design and other referenced HPM antennas were compared. As shown in Table 2, the proposed design has the advantages of wide-angle scanning and high gain in the frequency band of 7.5–8.5 GHz. The simulation and measurement results of the solid-state active phased array antenna proposed in this paper verify that the gain attenuation is small when it is scanned in two dimensions. Compared with other research, the proposed array antenna in practical application has a smaller size and occupied volume. At the same time, the proposed HPM solid-state active phased array has flexible space power synthesis capability, high directivity, and modularity advantages, which are observed from the comparison in Table 2. Compared with other references, this work achieved a smaller size and higher gain with the advantage of flexible beam scanning based on an MW-level power capacity. The antenna equipment proposed in [13,14] is very complex and bulky, while that in this paper has a more simple and practical antenna structure, and the array is modular, which means that it can be customized and reconfigurable in power synthesis. The power capacity per square meter can be calculated as 804.85 MW/m, which is far more than the power capacity proposed in [28,29]. In summary, the proposed high-power microwave antenna array has been verified to have higher gain and power capacity efficiency.

Table 2. The comparison of the proposed HPM active phased array antenna and other HPM antennas.

Reference	Frequency (GHz)	Gain (dB)	Size (mm × mm)	Scanning Angle	Power Capacity (MW)
[13]	8.4–10.8	23.4	\	±30°	358
[14]	9.6	30–30.3	\	±20°	233
[17]	30.4–30.9	25.8	117 × 30	\	50
[28]	9.2–9.75	26.3	2000 × 1500	±35°	96.5
[29]	1.8–2.4	23.14	260 × 1600	\	140
This work	7.5–8.5	27.5–27.9	250 × 280	±10°	56.34

The future research will pay more attention to the improvement of the unit power capacity of the high-power microwave active phased array. In fact, the huge industrial demand and application value of the active phased array for high-power microwave applications will be seen and described. The design of a mode converter and power divider

that are more in line with the index will be considered as the key point of the research on power capacity.

6. Conclusions

An X-band active phased array with flexible beam scanning for the high-power microwave was proposed for the first time. Compared with other high-power microwave array antennas, the proposed phased array antenna has the advantages of small size, simple structure, and high gain, which makes up for the shortcomings of the beam scanning antenna for high-power microwave applications. To match the impedance and suppress the generation of high-order modes, straight walls were added to improve impedance matching, and at the horn aperture the baffles were loaded to suppress higher-order modes and eliminate blind spots during beam scanning. Dual-port rectangular waveguide was proposed for the first time to increase the power capacity and reduce the profile height. The measured reflection coefficient bandwidth was 7.5–8.5 GHz, with an active VSWR less than 2. The measured gain of the proposed HPM antenna unit was 8.4–9.7 dB in the frequency range. The power capacity of the array was 56.34 MW. The phased array antenna has the characteristics of flexible scanning, small size, and high gain, and can be applied in high-power microwave systems.

Author Contributions: Conceptualization, R.L. and H.W.; methodology, N.W.; software, R.L.; validation, N.W., H.W. and R.Z.; formal analysis, R.L.; investigation, T.L.; resources, N.W.; data curation, R.L.; writing—original draft preparation, R.Z.; writing—review and editing, R.L.; visualization, N.W.; supervision, H.W.; project administration, H.W. All authors have read and agreed to the published version of the manuscript.

Funding: This research received no external funding.

Data Availability Statement: All data are included within the manuscript.

Conflicts of Interest: The authors declare no conflict of interest.

References

1. Barker, J.R.; Schamiloglu, E. *High Power Microwave Sources and Technology*; Wiley-IEEE Press: Piscataway, NJ, USA, 2001.
2. Benford, J. Space Applications of High-Power Microwaves. *IEEE Trans. Plasma Sci.* **2007**, *36*, 569–581. [[CrossRef](#)]
3. Zhang, J.; Ge, X.; Zhang, J.; He, J.; Fan, Y.; Li, Z.; Jin, Z.; Gao, L.; Ling, J.; Qi, Z. Research progresses on Cherenkov and transit-time high-power microwave sources at NUDT. *Matter Radiat. Extrem.* **2016**, *1*, 163–178. [[CrossRef](#)]
4. Courtney, C.C.; Baum, C.E. The coaxial beam-rotating antenna (COBRA): Theory of operation and measured performance. *IEEE Trans. Antennas Propag.* **2000**, *48*, 299–309. [[CrossRef](#)]
5. Courtney, C.C.; Voss, D.E.; Baum, C.E.; Prather, W.; Torres, R. A description and the measured performance of three coaxial beam-rotating antenna prototypes. *IEEE Antennas Propag. Mag.* **2002**, *44*, 30–47. [[CrossRef](#)]
6. Sun-Hong, M.; Hoe-Chun, J.; Gun-Sik, P.; Jihwan, A.; Joonho, S. Mode Conversion of High-Power Electromagnetic Microwave Using Coaxial-Beam Rotating Antenna in Relativistic Backward-Wave Oscillator. *IEEE Trans. Plasma Sci.* **2010**, *38*, 1391–1397. [[CrossRef](#)]
7. Yuan, C.-W.; Fan, Y.-W.; Zhong, H.-H.; Liu, Q.-X.; Qian, B.-L. A Novel Mode-Transducing Antenna for High-Power Microwave Application. *IEEE Trans. Antennas Propag.* **2006**, *54*, 3022–3025. [[CrossRef](#)]
8. Misilmanil, H.E.; Al-Husseini, M.; Kaban, Y.K.; EI-HAJJ, A. Improved Vlasov Antenna with Curved Cuts for High Power Microwaves. In Proceedings of the IEEE International Conference on High Performance Computing & Simulation, Helsinki, Finland, 1–5 July 2013; pp. 362–365.
9. Zhang, X.; Wang, Q.; Cheng, Y.; Wen, S. Design of a 220GHz Vlasov (antenna) mode converter. In Proceedings of the 2012 International Workshop on Microwave and Millimeter Wave Circuits and System Technology, Chengdu, China, 19–20 April 2012. [[CrossRef](#)]
10. Fazaelifar, M.; Fatorehchy, M.R. Design, Fabrication and Test of Parabolic Cylinder Reflector and Horn for Increasing the Gain of Vlasov Antenna. *Prog. Electromagn. Res. Lett.* **2008**, *4*, 191–203. [[CrossRef](#)]
11. Liang, Y.; Zhang, J.; Liu, Q.; Li, X. High-Power Dual-Branch Helical Antenna. *IEEE Antennas Wirel. Propag. Lett.* **2018**, *17*, 472–475. [[CrossRef](#)]
12. Li, X.-Q.; Liu, Q.-X.; Zhang, J.-Q.; Zhao, L. 16-Element Single-Layer Rectangular Radial Line Helical Array Antenna for High-Power Applications. *IEEE Antennas Wirel. Propag. Lett.* **2010**, *9*, 708–711. [[CrossRef](#)]
13. Kong, G.; Li, X.; Wang, Q.; Zhang, J. A Wideband Reconfigurable Dual-Branch Helical Reflectarray Antenna for High-Power Microwave Applications. *IEEE Trans. Antennas Propag.* **2020**, *69*, 825–833. [[CrossRef](#)]

14. Guo, L.; Huang, W.; Chang, C.; Li, J.; Liu, Y.; Meng, R. Studies of a Leaky-Wave Phased Array Antenna for High-Power Microwave Applications. *IEEE Trans. Plasma Sci.* **2016**, *44*, 2366–2375. [[CrossRef](#)]
15. Meng, R.; Xia, Y.; Guo, Y.; Zhu, Q. An X-Band 48-Way Leaky Waveguide Antenna with High Aperture Efficiency and High Power Capacity. *IEEE Trans. Antennas Propag.* **2018**, *66*, 6799–6809. [[CrossRef](#)]
16. Pan, X.; Christodoulou, C.G. A narrow-wall slotted waveguide antenna array for high power applications. In Proceedings of the 2014 IEEE Antennas and Propagation Society International Symposium (APSURSI), Memphis, TN, USA, 6–11 July 2014. [[CrossRef](#)]
17. Liu, L.; Yang, Y.; Li, S.; Fang, X.; Meng, F.; Yu, C. A 3D Printed Ka-Band High-Efficiency Wide-Slit Antenna Array for High-Power Microwave Applications. *Int. J. Antennas Propag.* **2022**, *2022*, 1–8. [[CrossRef](#)]
18. Ma, X.; Yang, F.; Yang, P.; Wang, R.; Yan, Y. Compact coaxial slotted-cavity feed antenna with shaped-beam pattern for high-power microwave using high-order modes and polarisation cancellation techniques. *IET Microw. Antennas Propag.* **2020**, *14*, 578–585. [[CrossRef](#)]
19. Yadav, S.V.; Chittora, A. A Compact High Power UWB TEM Horn Antenna. In Proceedings of the IEEE International Conference on Electronics, Computing and Communication Technologies (CONECCT), Bangalore, India, 2–4 July 2020; pp. 1–3.
20. Zhang, Q.; Yuan, C.; Liu, L. A coaxial corrugated dual-band horn feed. *IEEE Antennas Wirel. Propag. Lett.* **2009**, *8*, 1357–1359. [[CrossRef](#)]
21. Yadav, S.V.; Chittora, A. A compact ultra-wideband transverse electromagnetic mode horn antenna for high power microwave applications. *Microw. Opt. Technol. Lett.* **2021**, *63*, 264–270. [[CrossRef](#)]
22. Teniente, J.; Gonzalo, R.; del-Rio, C. Innovative High-Gain Corrugated Horn Antenna Combining Horizontal and Vertical Corrugations. *IEEE Antennas Wirel. Propag. Lett.* **2006**, *5*, 380–383. [[CrossRef](#)]
23. Wei, L.; XiaoLi, X. Design and Simulation of TEM Double Ridge Guide Horn Antenna. In Proceedings of the 8th International Conference on Electronic Measurement and Instruments, Xi'an, China, 16–18 August 2007.
24. Chang, C.; Zhu, X.; Liu, G.; Fang, J.; Xiao, R.; Chen, C.; Shao, H.; Li, J.; Huang, H.; Zhang, Q.; et al. Design and Experiments of the Gw High-Power Microwave Feed Horn. *Prog. Electromagn. Res.* **2010**, *101*, 157–171. [[CrossRef](#)]
25. Khan, A.M.; Ahmed, M.M.; Rafiq, M.; Rafique, U. Design of an Efficient High Power Microwave antenna. In Proceedings of the 19th International Multi-Topic Conference (INMIC), Jaipur, India, 13–16 December 2016. [[CrossRef](#)]
26. Liang, T.; Huang, W.; Shao, H.; Wang, K.; Li, J.; Huang, H. Design and near field characteristic of high power microwave dual-reflector antenna. In Proceedings of the 2012 International Conference on Microwave and Millimeter Wave Technology (ICMMT), Shenzhen, China, 5–8 May 2012; pp. 1–4.
27. Ma, X.; Yang, F.; Yang, P.; Wang, R.; Yan, Y. High-power and low-profile metamaterials for reflectarray based on ϵ -negative layer in X-band. *Electron. Lett.* **2020**, *56*, 172–174. [[CrossRef](#)]
28. Yu, L.-Z.; Yuan, C.-W.; He, J.-T.; Zhang, Q. Beam Steerable Array Antenna Based on Rectangular Waveguide for High-Power Microwave Applications. *IEEE Trans. Plasma Sci.* **2018**, *47*, 535–541. [[CrossRef](#)]
29. Xu, L.; Yuan, C.-W.; Zhang, Q.; Sun, Y.-F. Designs and experiments of a novel compact E-shaped wideband planar antenna array for high-power microwave application. *Rev. Sci. Instrum.* **2019**, *90*, 084703. [[CrossRef](#)] [[PubMed](#)]
30. Ng, J.; Ziolkowski, R.W.; Tyo, J.S.; Skipper, M.C.; Abdalla, M.D.; Martin, J. An Efficient, Electrically Small, Three-Dimensional Magnetic EZ Antenna for HPM Applications. *IEEE Trans. Plasma Sci.* **2012**, *40*, 3037–3045. [[CrossRef](#)]
31. Ramon, E.S.; Tyo, J.S.; Ziolkowski, R.W.; Skipper, M.C.; Abdalla, M.D.; Martin, J.M.; Altgilbers, L.L. A Compact Multi-Frequency, High Power Radiating System Combining Dual-Band, Electrically Small Magnetic EZ Antennas and Multi-Frequency Standing Wave Oscillator Sources. *IEEE Trans. Antennas Propag.* **2014**, *62*, 3281–3289. [[CrossRef](#)]